ACS Catalysis

Research Article

pubs.acs.org/acscatalysis

$MgCl_2 \cdot 6CH_3OH$: A Simple Molecular Adduct and Its Influence As a Porous Support for Olefin Polymerization

Edwin S. Gnanakumar,[†] Ravikumar R. Gowda,[‡] Shrikant Kunjir,[§] T. G. Ajithkumar,[§] P. R. Rajamohanan,[§] Debashis Chakraborty,[‡] and Chinnakonda S. Gopinath*[,†,⊥]

[†]Catalysis Division, [§]Central NMR Facility, [⊥]Center of Excellence on Surface Science, CSIR−National Chemical Laboratory, Dr. Homi Bhabha Road, Pune 411 008, India

[‡]Department of Chemistry, Indian Institute of Technology, Madras, Chennai 600 036, India

Supporting Information

ABSTRACT: A single phase molecular adduct, $MgCl_2 \cdot 6CH_3OH$ has been synthesized using $MgCl_2$ and the simplest alcohol, methanol. Structural, spectroscopic, and morphological studies have been carried out for a better understanding of the single phase $MgCl_2 \cdot 6CH_3OH$ adduct. ^{13}C CPMAS solid state NMR studies show all six methanol molecules are magnetically equivalent and present in a single environment around the Mg^{2+} center. Raman spectral analysis of the characteristic peak at 708 cm^{-1} substantiates octahedral coordination of six CH_3OH molecules around Mg^{2+}. Solid state ^{13}C NMR measurements, made after heat treatment at different temperatures, have been utilized to understand the variations in CH_3OH stoichiometry and coordination around Mg^{2+} with temperature. A titanated active catalyst, $TiCl_4$ on $MgCl_2 \cdot 6CH_3OH$, has also been synthesized and subjected to detailed characterizations. The active catalyst shows high surface area (102 m^2/g) and mesoporosity. The titanated catalyst has been screened for ethylene polymerization reactions using different cocatalysts (R_3Al; R= $-CH_3$, $-CH_2CH_3$, and $-CH_2CH(CH_3)_2$). A total of 7.25 kg of polyethylene per gram of catalyst has been obtained with Me_3Al cocatalyst, which is six times higher in activity compared with commercial $Me_3Al/TiCl_4/$ $MgCl_2 \cdot 6EtOH$-supported catalyst. Although porosity influences the catalytic activity, other factors also seem to contribute to the total catalytic activity.

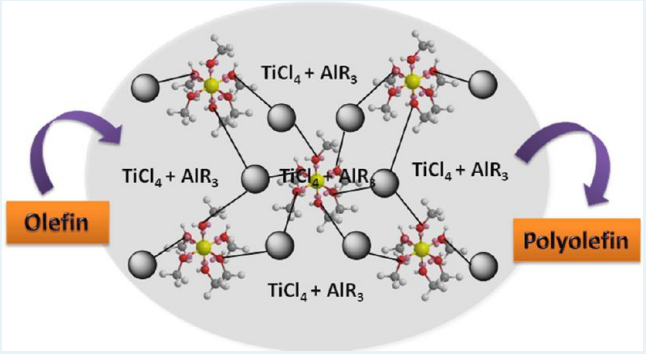

KEYWORDS: *molecular adduct, heterogeneous catalysis, Ziegler−Natta catalyst, olefin polymerization, $MgCl_2$*

1. INTRODUCTION

After the invention of the $TiCl_4$-derived polymerization catalyst by Ziegler and Natta in the 1950s, the growth of polyolefin industries was begun.[1−4] Discovery of activated $MgCl_2$ as a suitable support for the Ziegler−Natta (Z−N) catalyst in 1968 by Kashiwa again triggered evolution of the production of polyolefins.[5−7] In the ever steadily increasing polyolefin market, demand for polyethylene and polypropylene are satisfied by the polymerization reaction using the heterogeneous Z−N catalyst.[7] The components of the above Z−N catalyst generally consist of $TiCl_4$ as an active part, alkyl aluminum (R_3Al) as a cocatalyst, and $MgCl_2$ as a support. Apart from these three components, to increase the activity and stereospecificity of the catalyst, Lewis bases or electron donors (ED) such as alcohols, esters, and ethers have been added. The advantages of $MgCl_2$-supported Z−N catalysts are their extremely high activity and high isotactic index in stereospecific polymerization reactions.[7,8] Another benefit from a polymer product point of view is that, by controlling the porosity and morphology of the catalyst particle, we can tune the properties of the polymers obtained.[9−15]

Because of the vast industrial impact of the Z−N catalyst, theoretical[16−20] and experimental[21−26] efforts have been made to understand the active sites. Despite a significant amount of research, many aspects are yet to be properly understood about the Z−N catalyst: importantly, (a) the precise structure of the active sites on the specific surface of $MgCl_2$, (b) the exact role of electron donors on the activation of the $MgCl_2$ surface, (c) the nature of the electron donor and stoichiometry around $MgCl_2$ and its influence in the activity, and (d) the role of aluminum alkyl cocatalysts. Although the advantages of $MgCl_2$-supported catalysts are massive compared with other types of polymerization catalysts, the complexities present in the system boosts scientific understanding and thereby appropriate improvement in the catalyst design and development.[16,27−29] Much less scientific rationale was behind the advanced version of the supported Z−N catalyst because of the poor molecular level understanding aspects. From an industrial point of view, a

Received: November 12, 2012
Revised: January 13, 2013
Published: January 15, 2013

 © 2013 American Chemical Society

definite correlation between the structural and electronic structure of the catalyst support to the catalytic activity would primarily help the huge production of polyolefin business worldwide. Therefore, it is a great challenge to surface science, spectroscopy, and computational methods to elucidate the molecular aspects of the Mg-containing catalyst support to obtain better understanding of Z−N catalyst systems.[18,24−31]

The method of preparing the support, especially the nature of the molecular adduct and the alcohol employed, drastically influence the catalytic activity through porosity.[32−36] Indeed, a "*super active*" catalyst support, prepared from a molecular adduct between $MgCl_2$ and ethanol[29] or isopropyl alcohol,[34] has been reported in the literature. A Z−N catalyst support has been prepared by treating $MgCl_2$ with an alcohol. Although the preparation method is simple, a profound understanding of the control of alcohol molecules in the supporting material, $MgCl_2{\cdot}x$ROH, is decisive, since the productivity and isotacticity of the Z−N catalyst depends on the ROH/$MgCl_2$ ratio.[37,38] Today, ethanol has been used routinely as an activator for many industrial heterogeneous Z−N catalyst systems. In general, superactive catalyst synthesis involves removal of alcohols from the molecular adduct and simultaneous introduction of $TiCl_4$ into the $MgCl_2$ lattice to produce a porous nanostructure of the Z−N system, which influences the catalytic activity and the properties of the polymer obtained.[37−39] It is well understood that the nature of the alcohol in the $MgCl_2{\cdot}x$ROH predominantly decides the catalytic activity and, thus, the properties of the polymers; however, very few reports are available on the influence of different alcohols on the activity. Our group has been reporting in the recent past on these lines of research with different alcohol molecules, such as secondary, cyclic, and aromatic alcohols.[34−36,40,41]

Until now, theoretical research work has been focused on the interaction of $TiCl_4$ with the specific cut surfaces of α-$MgCl_2$. Consequently the structure of the $MgCl_2{\cdot}x$ROH support has a good influence on the insertion of $TiCl_4$ on the proper facet of $MgCl_2$.[42−44] It has been speculated that $MgCl_2{\cdot}x$ROH with different alcohols exposes different crystal planes of $MgCl_2$; hence, the variation in activity. In addition, the porous character of the $TiCl_4/MgCl_2$ catalyst is also important for its catalytic activity. Thus, a fair amount of knowledge about the structural aspects of $MgCl_2{\cdot}x$ROH precursor is required. To date, there have been only a few single crystal structures (namely, $MgCl_2{\cdot}6$EtOH (MgEtOH) and $MgCl_2{\cdot}6$BzOH) that have been made available in the literature among the molecular adducts, mainly because of the difficulties in preparing single crystals[45,46] Powder XRD and solid state NMR methods also provide significant structural details of these adducts. A detailed solid state NMR study of the ethanol adduct revealed the presence of mixed phases of $MgCl_2{\cdot}x$EtOH ($1 \leq x \geq 3$).[29] Crystal structures of $MgCl_2{\cdot}x$EtOH (x = 1.5, 2.8, and 3.3) have been resolved using an ab initio method from the data derived from high resolution X-ray powder diffraction.[47] Many such efforts are required for better understanding of the structural aspects of molecular adducts.

In this Article, we describe the synthesis of a single phase molecular adduct of $MgCl_2{\cdot}6CH_3OH$ (MgMeOH) as the supporting material. The simplest Lewis base with one carbon—namely, methanol—has been chosen to reduce the complexities during the characterization of the adduct as well as the final active catalyst. To the best of our knowledge, no detailed studies of $MgCl_2{\cdot}6CH_3OH$ are available in the literature.[48] For a deeper understanding of multicomponent complex systems of this type, which interact with each other, it is vital to identify the physicochemical properties of the individual components and to allow the complexities to increase linearly.[49] An active catalyst (Ti−MgMeOH) has been prepared, characterized and evaluated for polymerization activity. Both MgMeOH adduct and Ti−MgMeOH, the active catalyst, have been subjected to various structural, spectroscopic, and morphological characterizations to understand the system thoroughly. The Ti−MgMeOH catalyst shows much better activity compared with many other commercial catalysts based on Ti−MgEtOH Z−N catalysts.

2. EXPERIMENTAL SECTION

All the syntheses and reactions were performed under dry nitrogen atmosphere using standard Schlenk techniques. Partially hydrated (~5% H_2O) $MgCl_2$, titanium tetrachloride, dried methanol (from Sigma Aldrich), trimethylaluminium (TMA, 1.0 M solution in heptane), triethylaluminum (TEA, 0.6 M solution in heptane) and tri-isobutylaluminium (TIBA, 1.1 M solution in toluene) (from Acros Organics) were used as received. *n*-Hexane and toluene solvents (from Merck) were dried by refluxing with Na wire prior to use. Ethylene (purity of 99.99%) was taken from a commercial plant and used without further purification for ethylene polymerization. Chlorobenzene (Sigma−Aldrich) was used after drying over anhydrous calcium hydride.

2.1. Synthesis of $MgCl_2{\cdot}6CH_3OH$ (MgMeOH). MgMeOH adduct was synthesized using a well established azeotropic distillation method.[32,50] Partially hydrated $MgCl_2$ (0.1 M) and 1.2 M dried methanol were added in the required quantity of toluene in a 200 mL round-bottom flask. The above reaction mixture was refluxed under stirring for 3 h at 105 °C. Subsequently, the solution was kept at 0 °C for 3 h for crystallization of the MgMeOH adduct. The white precipitate was washed with 800 mL of hexane, dried at room temperature under vacuum for 30 min, and stored in a vacuum desiccator. The MgEtOH adduct was prepared by the procedure given in earlier publications.[34−36]

2.2. Titanation of $MgCl_2{\cdot}6CH_3OH$ Adduct (Ti−MgMeOH). Titanation of the MgMeOH adduct was carried out by following the procedures given in the literature, with the following minor modifications:[34,51] 28 g of MgMeOH adduct was added to 220 mL of chlorobenzene and stirred for 1 h at 110 °C. Subsequently, 220 mL of $TiCl_4$ was added over a period of 10 min, and the mixture was stirred for an additional 1 h. The resulting solid product was washed with two 100 mL portions of $TiCl_4$. Finally, the solid catalyst was filtered and washed several times with dry hexane at 60 °C until all the physisorbed Ti species was removed. The resulting Ti−MgMeOH catalyst was dried under vacuum and stored in a dry N_2 atmosphere. This procedure was adopted for the synthesis of the Ti−MgEtOH active catalyst.

2.3. Ethylene Polymerization. Polymerization of ethylene was carried out in a Buchi glasuster glass polyclave reactor fitted with a thermocouple, an automatic temperature control unit, and stirring speed of 500 rpm. In a typical polymerization, 0.5 L of dry hexane was added to the reactor at 75 °C, followed by alkyl aluminum (solution in *n*-heptane), and the catalyst was introduced into the reactor under a dry N_2 stream, and then the reactor was evacuated. Ethylene (5 bar) was then fed at a constant pressure. Polymerization was carried out for 1 h at 75 °C. An atmospheric pressure reaction was carried out in a glass reactor by continuously passing ethylene gas for 1 h at 75 °C.

dx.doi.org/10.1021/cs300730j | *ACS Catal.* 2013, 3, 303−311

2.4. Characterization Methods. The X-ray diffraction pattern was recorded on a Philips X'Pert Pro powder X-ray diffractometer using Cu Kα radiation (λ = 1.5418 Å) with a flat sample stage in the Bragg−Brentano geometry. The diffractometer was equipped with a Ni filter and X'celerator as the detector. All the samples were scanned between the range of 2θ = 5−75°. A thin layer of nujol on the sample surface was applied before recording the diffraction pattern to avoid the degradation of the sample by reaction with the atmosphere.[34,51,52] Thermal analysis of the adduct and its titanated catalyst were carried out using a Perkin-Elmer Diamond's thermogravimetry (TG) and differential thermal analysis (DTA) instrument using alumina as an internal standard.[34−36] Raman spectra were recorded on a Horiba JY Lab RAM HR 800 spectrometer excited with 633 nm lasers. While recording Raman measurements, to avoid any degradation of the materials, a low-temperature setup (Linkam-Examine-THMS 600 setup connected to a TP94 temperature programmer and LN94 unit to cool the stage below ambient temperature using liquid nitrogen) was employed.[53,54] The sample temperature was maintained below 0 °C to avoid any degradation from atmospheric moisture. A high-resolution FEI QUANTA 200 3D Environmental SEM was used to measure the surface morphology. Nova 1200 Quanta chrome equipment was used to measure the surface area by using Brunauer−Emmett−Teller (BET) method via nitrogen adsorption.[41]

All the solid state NMR experiments were carried out on a Bruker Avance 300 spectrometer operating at a static field of 7.04 T, resonating at 75.5 MHz for ^{13}C and 300 MHz for ^{1}H, using a 4 mm double resonance MAS probe.[55] Samples in the form of a fine powder were packed into a 4 mm o.d. zirconia rotor under nitrogen atmosphere and spun at 8 or 10 kHz. ^{13}C CPMAS measurements were performed using a standard ramped-amplitude cross-polarization pulse sequence.[56]The CPMAS experiments were carried out using a recycle delay of 4 s and a contact time of 2.5 ms. Chemical shifts were referred to the CH_2 carbon of adamantine (38.48 ppm) for ^{13}C. Typically, 4500 scans of transients were collected, and the sensitivity of the raw data was improved by exponential multiplication using a line broadening factor of 50 Hz.

Molecular weight distributions and polydispersities of polyethylene materials were determined using GPC (Waters 150-CALC/GPC) at 135 °C in 1,2,4-trichlorobenzene as solvent. μ-Styragel columns were used, and the peaks were calibrated with polystyrene. A 0.3−0.4% w/v solution was used at a flow rate of 1 mL/min.

3. RESULTS AND DISCUSSION

3.1. Characterization Method of Adduct. Figure 1 shows the powder XRD of anhydrous $MgCl_2$, MgEOH and MeMeOH adducts. The diffraction pattern of $MgCl_2$ corresponds to a rhombohedral crystal structure with cubic close packing that shows strong diffraction features at 2θ value of 15.1° (003) and 35° (004). The XRD pattern of MgMeOH adduct gives a high-intensity peak at a 2θ value of 11.9° (001) (d = 7.3238 Å) and 23.8° (002). Similarly, the XRD pattern of the MgEtOH adduct shows a strong diffraction pattern of the (001) plane at 2θ value of 9° (d = 9.8378 Å) and further diffractions at 18° (002) and 36° (004) characteristics for rhombohedral structure.[29,32,57] The selective high intensity of the (001), (002), and (004) planes are evident for the preferentially oriented (00l) growth of MgMeOH and MgEtOH adduct crystallites in the present azeotropic

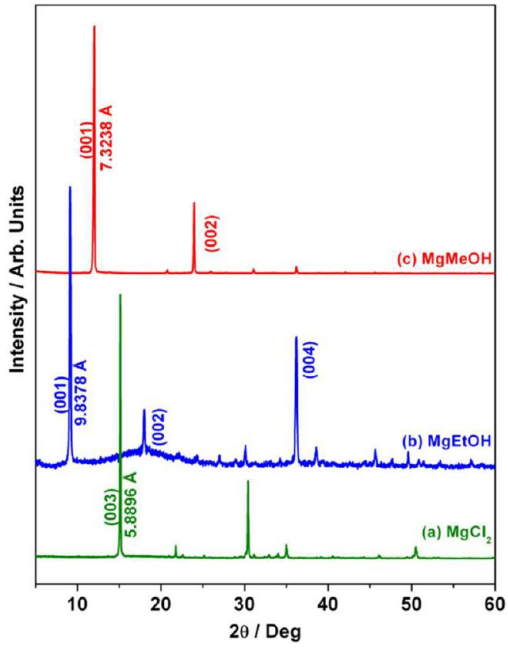

Figure 1. Powder X-ray diffraction pattern of (a) anhydrous $MgCl_2$, (b) MgEtOH, and (c) the MgMeOH adduct.

distillation preparation method. High-intensity (00l) planes characterize the growth of crystallites along the z-axis of the layered structure of $MgCl_2$ to form octahedral coordinated molecular adducts.[32] The smaller d value of the MgMeOH adduct compared with the MgEtOH adduct is directly correlated to the smaller size of methanol compared with ethanol.

Figure 2 shows the thermogravimetry and differential thermal analysis of the MgMeOH adduct. The temperature of the sample was ramped from ambient to 300 °C at 5 °C/min under flow of nitrogen (99.999%) at 40 mL/min. Well-defined sharp

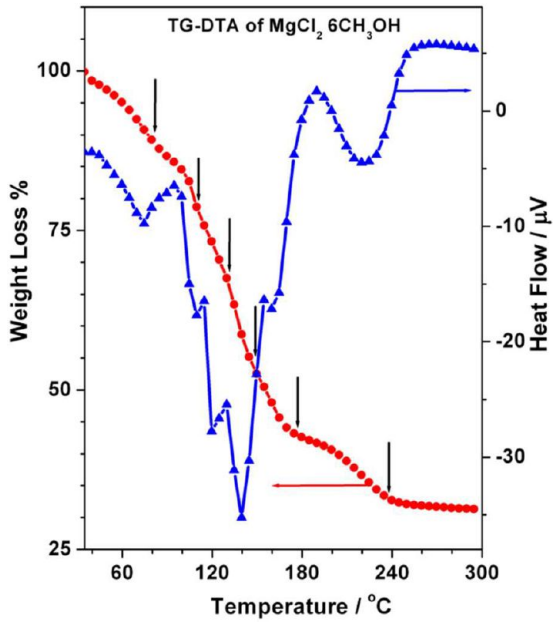

Figure 2. Thermal analysis of the MgMeOH adduct. The temperature was ramped from ambient to 300 °C at 5 °C/min under a flow of ultrapure N_2 at 40 mL/min.

dx.doi.org/10.1021/cs300730j | ACS Catal. 2013, 3, 303−311

DTA peaks and the associated weight loss indicate the systematic sequential dissociation of methanol molecules from the MgMeOH adduct.[32,34,36] The dissociation of the first methanol molecule occurs at 82 °C (which is above the boiling point of methanol, 65 °C) shows the interaction of methanol with $MgCl_2$ is strong. It is also to be noted that weight loss begins from 35 °C. Further, sharp weight loss occurs at 111, 130, 147, 176, and 235 °C because of the loss of second to sixth methanol molecules, respectively, in a stepwise manner. Weight loss >100 °C clearly indicates the methanol molecules bound strongly with $MgCl_2$. In addition, in DTA analysis, six different peaks/transitions are also observed, indicating the successive dealcoholation. Sharp and well-defined DTA peaks underscore the intramolecular interaction between the methanol molecules and $MgCl_2$. On the basis of the molecular formula $MgCl_2{\cdot}6CH_3OH$, the calculated weight loss is in excellent agreement with that of experimental weight loss observed (68%), within an error margin of ±1%. From the above calculation also, the ratio of MeOH/$MgCl_2$ has been derived to be six.

Raman spectra of anhydrous $MgCl_2$, MgMeOH adduct, and liquid methanol are shown in Figure 3. $MgCl_2$ has a

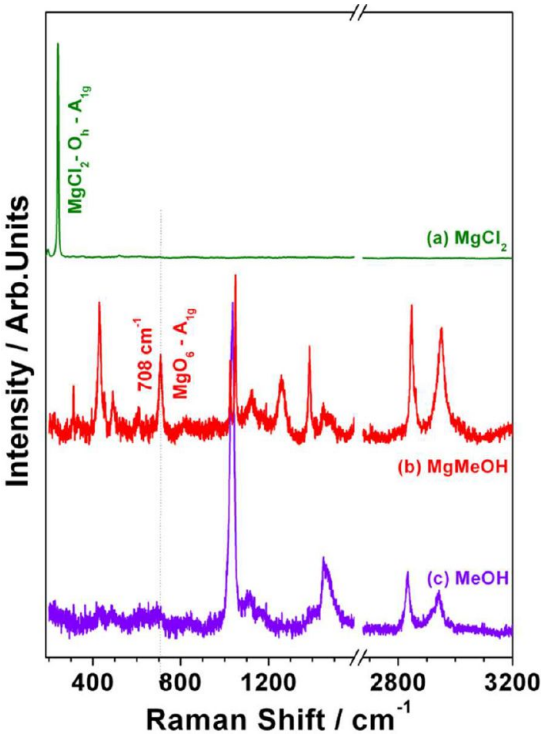

Figure 3. Raman spectra of (a) $MgCl_2$, (b) MgMeOH, and (c) MeOH.

rhombohedral structure with a D_{3d} space group and has a layered structure. The Mg^{2+} ion is coordinated to six chloride ions in the distorted octahedral geometry.[58,59] $MgCl_2$ shows a high, intense peak at 243 cm^{-1}, which has been assigned to the A_{1g} breathing mode of MgO_6 octahedra in the lattice. No other peaks were observed for $MgCl_2$. Liquid methanol shows a strong peak for C−O stretching at 1033 cm^{-1}, a medium peak for the $-CH_3$ bending mode at 1445 cm^{-1}, a −C−H symmetric stretching peak at 2832 cm^{-1}, and a −C−H antisymmetric peak at 2941 cm^{-1}.[60] The adduct, MgMeOH, shows an extra peak at 708 cm^{-1}, in addition to the features observed for neat methanol. This specific Raman mode indicates the formation of a Mg−O bond between $MgCl_2$ and the alcoholic oxygen to form a MgO_6 octahedron.[40,41,59] There is a significant shift in the above Raman feature compared with MgEtOH (684 cm^{-1}), and it is attributed to the change in electronic and structural features of MgMeOH and MgEtOH. It is speculated that MeOH interacts more strongly with $MgCl_2$ than withEtOH.

The ^{1}H MAS spectrum of MgMeOH (Figure 4a) shows both broad and narrow features. Two narrow peaks are observed at

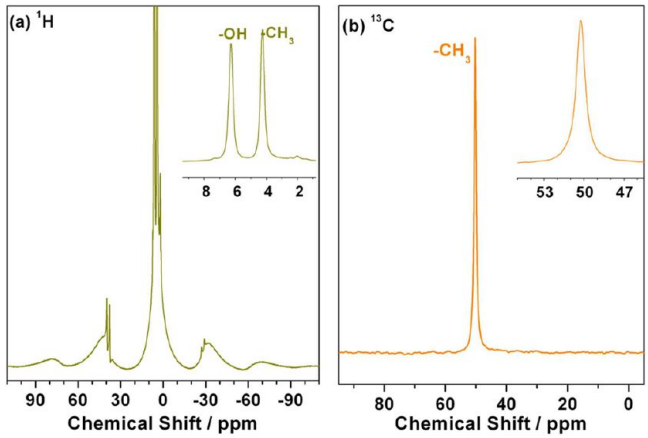

Figure 4. (a) ^{1}H MAS and (b) ^{13}C CPMAS NMR spectrum of MgMeOH.

4.2 and 6.3 ppm for the MgMeOH adduct, indicating the presence of protons from $-CH_3$ and $-OH$, respectively. The ^{13}C CPMAS spectrum (Figure 4b) of the MgMeOH adduct shows a single peak at 50.2 ppm. The absence of splitting in the ^{13}C peak clearly shows the presence of only one type of carbon in MgMeOH. From the ^{13}C CPMAS spectrum, we could conclude that the MgMeOH has been prepared in a single phase. ^{13}C single pulse excitation MAS spectrum of MgMeOH also exhibited (data not shown) only one environment at 50.2 ppm.

Figure 5 shows the ^{1}H MAS NMR and ^{13}C CPMAS spectra of the MgMeOH adduct recorded at room temperature and after heating at different temperatures for 1 h under N_2 flow. As the heating temperature increases, the number of peaks

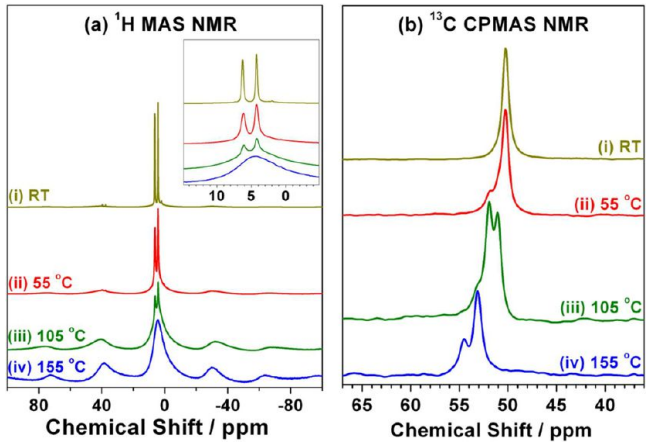

Figure 5. (a) ^{1}H MAS and (b) ^{13}C CPMAS NMR spectra recorded at RT, after heat treatment of MgMeOH at different temperatures given on the traces.

dx.doi.org/10.1021/cs300730j | ACS Catal. 2013, 3, 303−311

observed in the ^{13}C CPMAS spectrum also increases as a result of loss of symmetry and also shows a downfield shift. The profile and the chemical shift of MgMeOH are significantly affected by heating at different temperatures because of the removal of methanol from the MgMeOH adduct. The complexity of the spectrum has increased due to the nonequivalence of CH_3OH molecules present around Mg^{2+} after the ex situ heating. As the temperature increases, the $MeOH/MgCl_2$ ratio starts to decrease as a result of the increasing extent of dealcoholation at higher temperature. Temperatures chosen were based on the observations made from TG−DTA data.

A closer look at these ^{13}C CPMAS data, without any background correction (shown in Figure S1, Supporting Information) provides more insight to the nature of methanol molecules in the adduct after ex situ heating. On heating at 55 °C, the major signal found (∼70%) still corresponds to the hexa adduct at 50.25 ppm. In addition, these two additional weak signals of nearly equal intensity also appear at 51.01 and 51.90, indicting the presence of mixed phases. The intensity of the signals corresponding to the latter environment increased while the signal corresponding to the hexa adduct completely vanished on heating at 105 °C. At this stage, a new weak signal (10%) at 53.15 ppm also emerged, which became stronger at 155 °C. Yet another additional signal (∼30%) was also noticed at this temperature. It is very evident from the observed multiplicities and intensities of the ^{13}C signals that the system exists as mixed phases and the their populations vary with the thermal history. It is to be noted that downfield peaks are observed for lower coordination of methanol around Mg^{2+} due to a stronger degree of association. Similar observations were also noticed for the MgEtOH.[29] The TG−DTA results indicated that the number of CH_3OH coordinating around Mg^{2+} decreases gradually to ∼2 after heating at 155 °C, and hence, a substantial change in structure and electronic structure is expected.[61] A detailed investigation is required for proper understanding of the various phases of the adducts present during the process of dealcoholation.

The effects of loss of methanol from the adduct are further corroborated in the ^1H MAS NMR spectra (Figure 5a) collected after different extents of heating. The sharper features observed for the hexamethanolate (MgMeOH) adduct broadens on an increase in the temperature after heating and becomes very broad in the sample heat-treated at 155 °C. Alcohol molecules that are relatively more mobile in $MgCl_2{\cdot}6CH_3OH$ will have a stronger association with the matrix in $MgCl_2{\cdot}xCH_3OH$ when x tends to be less than 6. This increase in the strength of association is reflected as an increase in the ^1H line width, and for the sample heated at 155 °C, the molecular motions of methanol molecules in the adduct are arrested to a greater extent and, hence, exhibit very broad ^1H signal (tens of kilohertz), similar to the one associated with rigid molecules.

The compositions of various heat-treated MgMeOH adducts were measured by dissolving a known amounts of adduct in THF.[29,35,36] $MeOH/MgCl_2$ stoichiometry decreases from 6 for the parent adduct to 5.6, 2.9, and 1.3 after heat treatment at 55, 105, and 155 °C, respectively. It is to be noted that at a stoichiometry of 5.6, NMR results demonstrate the presence of two other phases along with the parent adduct and demonstrate a high sensitivity toward finding different compositions. A similar linear variation in the stoichiometry has been observed in TG−DTA results (Figure 2). The above stoichiometry measured changes are in good agreement with that of the results obtained in Figure 5, suggesting interaction between $MgCl_2$ and MeOH increases when the stoichiometry decreases. Similar findings were reported for $MgCl_2{\cdot}6EtOH$ adduct by Sozzani et al,[29] and it is worth exploring with detailed NMR measurements.

Scanning electron microscope (SEM) images of the MgMeOH adduct are shown in Figure 6. The images in Figure 6a and b were recorded after dispersing the MgMeOH adduct in anhydrous hexane.[35] It is evident that agglomerated particles with large distribution sizes are present in the MgMeOH adduct. The images in Figure 6c and d were recorded by dispersing the adduct in toluene−triblock copolymer solution to avoid agglomeration.[35,36] The SEM images clearly show particles with an average size of ∼5 μm. Close observation of the SEM image of the MgMeOH particles indicates that the surface is not uniformly spherical.

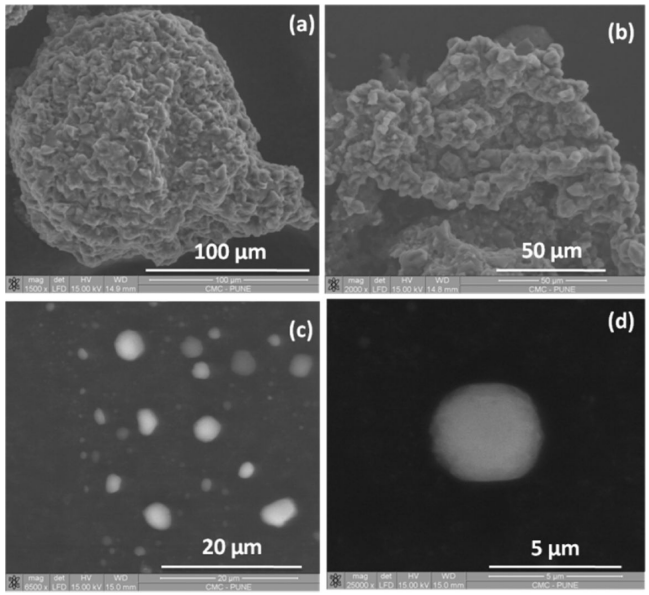

Figure 6. Scanning electron microscope image of the MgMeOH adduct. All the images were recorded at 15 KV. Magnification factors for a−d are 1500, 2000, 6500, and 25000, respectively.

3.2. Characterization of Titanated Adduct. Powder X-ray diffraction of Ti−MgMeOH active catalyst is shown along with anhydrous $MgCl_2$ and MgMeOH adduct in Figure 7. After $TiCl_4$ treatment, the characteristic peaks for the MgMeOH adduct completely disappear and broad diffraction features appear around 15°, 29−33°, and 50°. Because of the removal of methanol molecules from MgMeOH, a drastic change occurs from the highly oriented crystalline nature of the MgMeOH adduct into the $TiCl_x$-incorporated nanocrystalline $MgCl_2$ catalyst.[15,35,36,62] The broad, low-intensity peak around 15°(003) is due to the stacking of −Cl−Mg−Cl− triple layers along the crystallographic directions. This also signifies that the triple layer structure is severely ruptured, mainly to incorporate $TiCl_x$ in the $MgCl_2$ unit. The particle size of MgMeOH, measured from the SEM results shown in Figure 6 is ∼5 μm; however, the crystallite size, calculated by the Scherrer equation from the XRD results in Figure 7, is 14 nm for Ti−MgMeOH. The above size reduction is attributed to the change in long-range order on the MgMeOH adduct to short-range order after titanation. Stacking faults in the triple layers could be identified

dx.doi.org/10.1021/cs300730j | ACS Catal. 2013, 3, 303−311

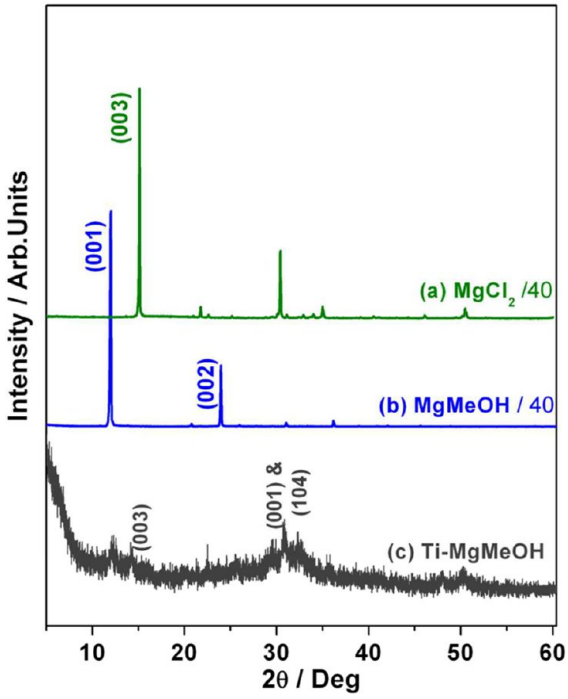

Figure 7. Powder X-ray diffraction of (a) $MgCl_2$, (b) the MgMeOH adduct, and (c) the Ti−MgMeOH active catalyst.

further by a halo, broad peak between 29° and 33° and a peak around 50°. A similar kind of XRD is reported for titanated catalyst in the literature, clearly indicating the highly disordered δ-$MgCl_2$ crystallographic form.[62,63]

The solid state NMR spectrum of the active catalyst is shown in Figure 8. Figure 8a shows ^{1}H MAS NMR of the Ti−MgMeOH active catalyst. The peak at 8 ppm indicates the presence of physisorbed chlorobenzene, which has been used in the preparation of the active catalyst for washing away any extra $TiCl_4$. A broad peak is observed between 6 and 4 ppm that is attributed to methanol and other small organic molecules trapped in the pores of the Ti−MgMeOH during the active catalyst synthesis. The broadness of the peak is due to the highly restricted motion of the molecules in the pores of the active catalyst. Another peak around 1.7 ppm is due to the trapped hydrocarbon present in the pores of the active catalyst.

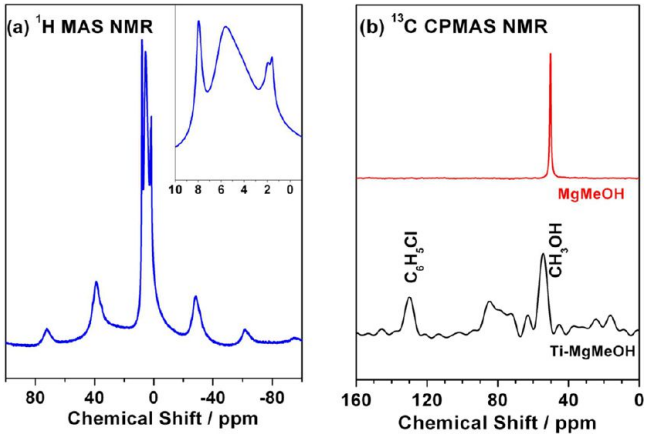

Figure 8. (a) ^{1}H and (b) ^{13}C CPMAS NMR spectra of the Ti−MgMeOH active catalyst.

The ^{13}C CPMAS NMR of the titanated catalyst is shown in Figure 8b. The peak observed at 130 ppm confirms the presence of chlorobenzene. Apart from this peak, a few more peaks are observed at 84, 54, and 20−15 ppm. During the preparation of Z−N catalysts, $TiCl_4$ interacts with MgMeOH, and there are chances for formation of HCl and CH_3OH and many cascade reactions involving either or both HCl and CH_3OH. This lead to formation of small molecules such as ethers, chlorinated methanol/ether, etc. trapped in pores. The peaks observed in the region 90−70 ppm are attributed to oxygenated species such as CH_3-O-CH_3, $Cl-CH_2OH$, or $Cl-CH_2-O-CH_3$ molecules formed during the above synthesis of Ti−MgMeOH. A peak at 54 and 20−15 ppm indicates free methanol molecules and hexane molecules adsorbed inside the pores of the active catalyst, respectively.

TG and DTA analyses of the Ti−MgMeOH catalyst are shown in Figure 9. Significant differences have been observed in the TG and DTA of MgMeOH adduct and the active catalyst, Ti−MgMeOH. First, the weight loss obtained in Ti−MgMeOH was 38%, compared with 68% in the case of MgMeOH. This net weight loss difference could be due to the removal of most of the methanol during the active catalyst preparation. As discussed in solid state NMR analysis of active catalyst, trapped organic molecules, such as chlorobenzene, hexane, ethers, and chlorinated CH_3OH molecules in the pores, seem to desorb during the ramping in TG−DTA and lead to weight loss.

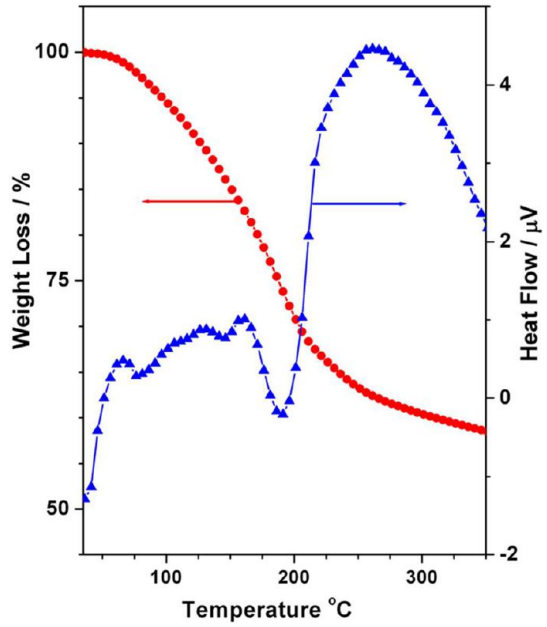

Figure 9. Thermal analysis of the Ti−MgMeOH active catalyst. The temperature was ramped from ambient to 300 °C at 5 °C/min under a flow of ultrapure N_2 at 40 mL/min.

Figure 10 shows the SEM images of the Ti−MgMeOH active catalyst. The images were recorded after the sonication of dispersed Ti−MgMeOH catalyst in triblock copolymer and toluene solution to avoid any agglomeration[40] and to resist the atmospheric degradation due to the air-sensitive nature of the catalyst. The SEM image clearly shows the highly porous nature of the catalyst.

The BET method was used to measure the surface area of the Ti−MgMeOH active catalyst from N_2 adsorption−desorption isotherm analysis; the results are shown in Figure 11. The

dx.doi.org/10.1021/cs300730j | ACS Catal. 2013, 3, 303−311

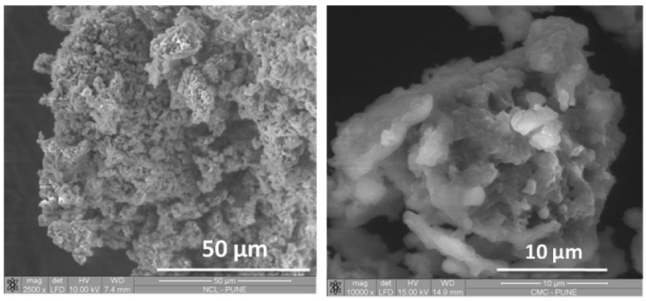

Figure 10. SEM image of Ti−MgMeOH active catalyst. Images were recorded at 10 (left) and 15 KV (right), respectively. Magnification factors for a and b are 2500 and 10000, respectively.

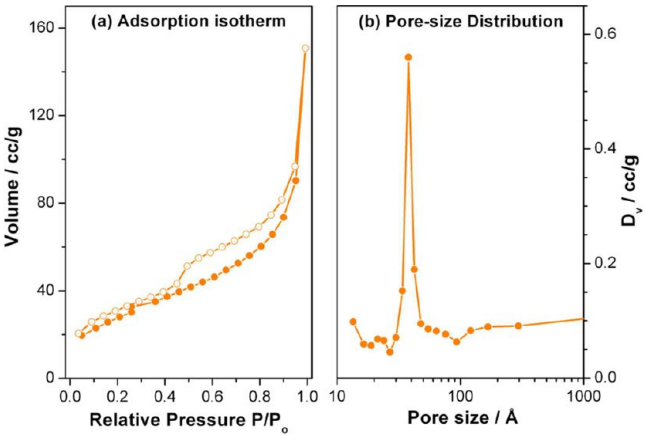

Figure 11. (a) Adsorption isotherm and (b) pore size distribution of the Ti−MgMeOH catalyst.

surface area of the active catalyst was 102 m^2/g which is higher than many commercial Ti-MgEtOH catalysts (32 m^2/g). The average pore diameter of Ti−MgMeOH was calculated, from the desorption branch of the adsorption isotherm, to be 41 Å, with a pore volume of 0.233 $cm^3\ g^{-1}$. However, the average pore diameter calculated from the adsorption branch is 2.4 nm, with a pore volume of 0.223 $cm^3\ g^{-1}$. The above difference is due to the sudden desorption in the isotherm around P/P_0 = 0.45 (Figure 11a).[64] Careful analysis of the adsorption isotherm indicates a type-IV (H3) isotherm[65] for the Ti−MgMeOH catalyst. It clearly shows the presence of predominant micropores along with mesopores in the Ti−MgMeOH catalytic system.

3.3. Ethylene Polymerization. Ethylene polymerization reactions were carried out using the Ti−MgMeOH catalyst, and cocatalysts with three different alkyl chains; namely, methyl, ethyl, and isobutyl (R_3Al; R = CH_3, $-CH_2CH_3$, and $-CH_2CH(CH_3)_2$). For each cocatalyst, reactions were carried out at two different pressures and at 75 °C. Polymerization results are shown in Table 1. Average results were taken after carrying out three sets of polymerizations for each condition. (1) As expected, higher activity of the catalyst was observed for the reaction carried out at a higher ethylene pressure (5 atm) compared with the 1 atm reaction. (2) Among the reactions with different catalysts, entry 4 shows the best ethylene polymerization activity of Ti−MgMeOH catalyst when Me_3Al was used as a cocatalyst at 5 atm. This activity is much higher compared with a commercial Ziegler−Natta catalyst (~6 times). (3) Indeed, at ambient pressure, polymerization at 75 °C with Ti−MgMeOH is greater than commercial catalyst activity at 5 atm pressure. Ti−MgMeOH activity was much higher than reported for the active catalyst derived from cyclohexanol.[41] (4) The higher activity of the Ti−MgMeOH−Me_3Al combination compared with the other cocatalyst combination could be due to narrow pores, which help the cocatalyst to interact with $TiCl_x$ species present inside the pores of the active catalyst. (5) The PE yield from Ti−MgMeOH catalyst is higher with Me_3Al; however, the MWD of PE is significantly higher with other cocatalysts. This could be due to the labile nature or higher reactivity of Me_3Al compared with other cocatalysts.

It is also to be emphasized that in addition to the porosity of the final catalyst, many other parameters seem to influence the catalytic activity and, hence, polyolefin yield. For example, Z−N catalyst derived from cyclohexanol adduct, entry 9, shows a significantly higher porosity (BET surface area 236 m^2/g and 11.8 nm pore diameter)[41] than that of methanol adduct-derived Z−N catalyst. Indeed, the above observation highlights the necessity of porosity for better activity; however, this alone is not sufficient. Furthermore, a different porosity likely leads to different crystallographic planes and, hence, interaction between $TiCl_x$ and $MgCl_2$, which in turn influences the mode of interaction with the cocatalysts.[66] Another likely possibility is the over reduction of catalytically active Ti species; because of higher porosity, the cocatalyst can interact with the Ti species and reduces to the undesirable Ti^{2+}. This type of electronic interaction would lead to a decrease in activity, despite the high surface area. In fact, a thorough study could lead to tunable properties of the Z−N catalyst system for olefin oligomerization to polymerization.

Table 1. Ethylene Polymerization Results of Using Ti−MgMeOH Catalyst[a]

S no.	support	Ti wt % (mmol)	cocatalyst	conditions	PE yield (g/g of catalyst)	PE yield (g/mmol of Ti)	Mn (M_w) g mol^{-1}	MWD
1	MgMeOH	13 (0.27)	Me_3Al	75 °C, 1 atm	3247	1208.80	10490 (140569)	13.4
2	MgMeOH	13 (0.27)	Et_3Al	75 °C, 1 atm	1863	693.56	12746 (150410)	11.8
3	MgMeOH	13 (0.27)	iBu_3Al	75 °C, 1 atm	1230	457.9	13985 (135660)	9.7
4	MgMeOH	13 (0.27)	Me_3Al	75 °C, 5 atm	7245	3188.65	26723 (275339)	10.3
5	MgMeOH	13 (0.27)	Et_3Al	75 °C, 5 atm	4588	1707.83	28113 (254141)	9.04
6	MgMeOH	13 (0.27)	iBu_3Al	75 °C, 5 atm	3199	1190.93	17334 (154273)	8.9
7	MgEtOH[34]	11 (0.23)	Et_3Al	75 °C, 5 atm	1300	572	22173 (255010)	11.5
8	MgBzOH[35]	24 (0.51)	Et_3Al	75 °C, 5 atm	960	183	26111 (188000)	7.2
9	MgCyOH[41]	9 (0.19)	iBu_3Al	75 °C, 5 atm	3570	1918	45801 (297710)	6.5

[a]Catalyst quantity = 0.1g; Al/Ti = 200, 50, 10, and 50 for MgMeOH, MgEtOH, MgBzOH, and MgCyOH, respectively.

dx.doi.org/10.1021/cs300730j | ACS Catal. 2013, 3, 303−311

4. CONCLUSION

Single phase MgMeOH adduct and its active catalyst Ti–MgMeOH were synthesized and subjected to detailed structural and spectroscopic investigations. The crystal structure of the MgMeOH adduct belongs to a rhombohedral with layered structure, whereas a highly disordered δ-$MgCl_2$ nanocrystalline structure has been observed for Ti–MgMeOH. Six methanol molecules are present in a magnetically equivalent environment around the Mg^{2+} in an octahedron environment. Variable temperature NMR experiments demonstrate the changing stoichiometry of the adduct and, induced, structural alterations. The textural properties of the active catalyst show the presence of a maximum of mesopores and a high surface area with an optimum amount of $TiCl_x$ species on the surface. The ethylene polymerization reaction shows 6 times better activity with Ti–MgMeOH compared to a commercial catalyst under comparable conditions. The higher activity of the Ti–MgMeOH catalyst with Me_3Al could be due to the easy accessibility of cocatalyst to the active Ti^{n+} species due to the mesoporous nature of the active catalyst.

■ ASSOCIATED CONTENT

Ⓢ Supporting Information

Figure 5 is given without background correction in Supporting Information as Figure S1. This material is available free of charge via the Internet at http://pubs.acs.org.

■ AUTHOR INFORMATION

Corresponding Author

*Phone: 0091-20-2590 2043. E-mail: cs.gopinath@ncl.res.in.

Notes

The authors declare no competing financial interest.

■ ACKNOWLEDGMENTS

E.S.G. thanks the Council of Scientific and Industrial Research (CSIR), New Delhi for a Senior Research Fellowship.

■ REFERENCES

(1) Ziegler, K.; Holzkamp, E.; Breil, H.; Martin, H. *Angew. Chem.* **1955**, *67*, 541.
(2) Ziegler, K.; Holzkamp, E.; Breil, H.; Martin, H. *Angew. Chem.* **1955**, *67*, 426.
(3) Natta, G. *J. Polym. Sci.* **1955**, *16*, 143.
(4) Natta, G.; Pino, P.; Corradini, P.; Danusso, F.; Mantica, E.; Mazzanti, G.; Moraglio, G. *J. Am. Chem. Soc.* **1955**, *77*, 1708.
(5) Kashiwa, N.; Fujimura, H.; Tokuzumi, Y. JP Patent 1031698, 1968.
(6) Kashiwa, N. *Polym. J.* **1980**, *12*, 603.
(7) Kashiwa, N. *J. Polym. Sci., Part A: Polym. Chem.* **2004**, *42*, 1.
(8) Kashiwa, N.; Yoshitake. *J. Makromol. Chem., Rapid Commun.* **1983**, *4*, 41.
(9) Hock, C. W. *J. Polym. Sci., Polym. Chem.* **1966**, *4*, 3055.
(10) Boor, J., Jr. *Ziegler-Natta Catalysts and Polymerization*; Academic Press: New York, 1979.
(11) Hutchinson, R. A.; Ray, W. H. *J. Appl. Polym. Sci.* **1991**, *43*, 1271.
(12) Galli, P. *J. Macromol. Sci., Phys., B* **1996**, *35*, 427.
(13) McKenna, T. F.; Soares, J. P. B. *Chem. Eng. Sci.* **2001**, *56*, 3931.
(14) Cecchin, G.; Morini, G.; Pelliconi, A. *Macromol. Symp.* **2001**, *173*, 195.
(15) Auriemma, F.; De Rosa, C. *Chem. Mater.* **2007**, *19*, 5803.
(16) Busico, V.; Causa, M.; Cipullo, R.; Credendino, R.; Cutillo, F.; Friederichs, N.; Lamanna, R.; Segre, A.; Castellit, V. V. *J. Phys. Chem. C.* **2008**, *112*, 1081.
(17) Monaco, G.; Toto, M.; Guerra, G.; Corradini, P.; Cavallo, L. *Macromolecules* **2000**, *33*, 8953.
(18) Boero, M.; Parrinello, M.; Terakura, K. *Surf. Sci.* **1999**, *438*, 1.
(19) Seth, M.; Margl, P. M.; Ziegler, T. *Macromolecules* **2002**, *35*, 7815.
(20) Stukalov, D. V.; Zakharov, V. A. *J. Phys. Chem. C* **2009**, *113*, 21376.
(21) Di Noto, V.; Fregonese, D.; Marigo, A.; Bresadola, S. *Macromol. Chem. Phys.* **1998**, *199*, 633.
(22) Mori, H.; Sawada, M.; Higuchi, T.; Hasebe, K.; Otsuka, N.; Terano, M. *Macromol. Rapid Commun.* **1999**, *20*, 245.
(23) Kim, S. H.; Somorjai, G. A. *Proc. Natl. Acad. Sci. U.S.A.* **2006**, *103*, 15289.
(24) Andoni, A.; Chadwick, J. C.; Milani, S.; Niemantsverdriet, H.; Thüne, P. C. *J. Catal.* **2007**, *247*, 129.
(25) Potapov, A. G.; Bukatov, G. D.; Zakharov, V. A. *J. Mol. Catal. A: Chem.* **2010**, *316*, 95.
(26) Brambilla, L.; Zerbi, G.; Piemontesi, F.; Nascetti, S.; Morini, G. *J. Phys. Chem. C* **2010**, *114*, 11475.
(27) Sobota, P. *Coord. Chem. Rev.* **2004**, *248*, 1047.
(28) Kim, S. H.; Somorjai, G. A. *J. Phys. Chem. B* **2002**, *106*, 1386.
(29) Sozzani, P.; Bracco, S.; Comotti, A.; Simonutti, R.; Camurati, I. *J. Am. Chem. Soc.* **2003**, *125*, 12881.
(30) Kim, S. H.; Craig, R. T.; Somorjai, G. A. *Langmuir* **2000**, *16*, 9414.
(31) Boero, M.; Parrinello, M.; Terakura, K. *J. Am. Chem. Soc.* **1998**, *120*, 2746.
(32) Bart, J. C. *J. Mater. Sci.* **1995**, *30*, 2809.
(33) Yang, C. B.; Hsu, C. C. *Polym. Bull.* **1993**, *30*, 52.
(34) Thushara, K. S.; Mathew, R.; Ajithkumar, T. G.; Rajamohanan, P. R.; Bhaduri, S.; Gopinath, C. S. *J. Phys. Chem. C* **2009**, *113*, 8556.
(35) Gnanakumar, E. S.; Thushara, K. S.; Bhange, D. S.; Mathew, R.; Ajithkumar, T. G.; Rajamohanan, P. R.; Bhaduri, S.; Gopinath, C. S. *Dalton Trans.* **2011**, *40*, 10936.
(36) Thushara, K. S.; Gnanakumar, E. S.; Mathew, R.; Ajithkumar, T. G.; Rajamohanan, P. R.; Bhaduri, S.; Gopinath, C. S. *Dalton Trans.* **2012**, *41*, 11311.
(37) Moore, E. P., Jr. *The Rebirth of Polypropylene: Supported Catalysts*; Hanser Publishers: New York, 1998, pp 45–71.
(38) Albizzati, E.; Giannini, U.; Collina, G.; Noristi, L. In *Polypropylene Handbook: Polymerization, Characterization, Properties, Applications*; Moore, E. P., Jr., Ed.; Hanser Publishers: New York, 1996, pp 11–111.
(39) Forte, M. C.; Coutinho, F. M. B. *Eur. Polym. J.* **1996**, *32*, 223.
(40) Thushara, K. S.; Gnanakumar, E. S.; Mathew, R.; Jha, R. K.; Ajithkumar, T. G.; Rajamohanan, P. R.; Sarma, K.; Padmanabhan, S.; Bhaduri, S.; Gopinath, C. S. *J. Phys. Chem. C* **2011**, *115*, 1952.
(41) Gnanakumar, E. S.; Thushara, K. S.; Gowda, R. R.; Raman, S. K.; Ajithkumar, T. G.; Rajamohanan, P. R.; Chakraborty, D.; Gopinath, C. S. *J. Phys. Chem. C.* **2012**, *116*, 24115.
(42) Seenivasan, K.; Sommazzi, A.; Bonino, F.; Bordiga, S.; Groppo, E. *Chem.—Eur. J.* **2011**, *17*, 8648.
(43) Buscio, V.; Corradini, P.; Martino, L.; Proto, A.; Savino, V. *Makromol. Chem.* **1985**, *186*, 1279.
(44) Correa, A.; Piemontesi, F.; Morini, G.; Cavallo, L. *Macromolecules* **2007**, *40*, 9181.
(45) Sacchi, M. C.; Forlini, F.; Tritto, I.; Mendichi, R.; Zannoni, G. *Macromolecules* **1992**, *25*, 5914.
(46) Valle, G.; Baruzzi, G.; Paganetto, G.; Depaoli, G.; Zannetti, R.; Marigo, R. *Inorg. Chim. Acta* **1989**, *156*, 157.
(47) Di Noto, V.; Bresadola, S.; Zannetti, R.; Viviani, M. *Z. Kristallogr.* **1993**, *204*, 263.
(48) Magalhase, D. N. T.; Filho, O. D. C.; Coutinho, F. M. B. *Eur. Polym. J.* **1991**, *27*, 827.
(49) Malizia, F.; Fait, A.; Cruciani, G. *Chem.—Eur. J.* **2011**, *17*, 13892.
(50) Sergeev, S. A.; Bukatov, G. D.; Zakharov, V. A; Moroz, E. M. *Makromol. Chem.* **1983**, *184*, 2421.

(51) Bhaduri, S.; Gupta, V. K. U.S. Patent 6841633, 2005; and references therein.
(52) Vijayaraj, M.; Gopinath, C. S. *J. Catal.* **2006**, *241*, 83.
(53) Mapa, M.; Thushara, K. S.; Saha, B.; Chakraborty, P.; Janet, C. M.; Viswanath, R. B.; Nair, C. M.; Murty, K. V. G. K.; Gopinath, C. S. *Chem. Mater.* **2009**, *21*, 2973.
(54) Maity, N.; Rajamohanan, P. R.; Ganapathy, S.; Gopinath, C. S.; Bhaduri, S.; Lahiri, G. K. *J. Phys. Chem. C* **2008**, *112*, 9428.
(55) Mathew, T.; Sivaranjani, K.; Gnanakumar, E. S.; Yamada, Y.; Kobayashi, T.; Gopinath, C. S. *J. Mater. Chem.* **2012**, *22*, 13484.
(56) Metz, G.; Wu, X.; Smith, O. S. *J. Magn. Reson., Ser. A* **1994**, *110*, 219.
(57) Xu, R.; Liu, D.; Wang, S.; Wang, N.; Mao, B. *J. Mol. Catal. A: Chem.* **2007**, *263*, 86.
(58) Ye, Z.-Y.; Wang, L.; Feng, L.-F.; Gu, X.-P.; Chen, H.-H.; Zhang, P.-Y.; Pan, J.; Jiang, S.; Feng, L.-X. *J. Polym. Sci., Part A: Polym. Chem.* **2002**, *40*, 3112.
(59) Tewell, C. R.; Malizia, F.; Ager, J. W., III; Somorjai, G. A. *J. Phys. Chem. B* **2002**, *106*, 2946.
(60) Balasubrahmanyam, K. *J. Chem. Phys.* **1966**, *44*, 3270.
(61) (a) Sivaranjani, K.; Verma, A.; Gopinath, C. S. *Green Chem.* **2012**, *14*, 461. (b) Murugan, B.; Ramaswamy, A. V.; Srinivasa, D.; Gopinath, C. S.; Ramaswamy, V. *Chem. Mater.* **2005**, *17*, 3983.
(62) Ronkko, H. L.; Knuutilla, H.; Denifl, P.; Leinonen, T.; Venalainen, T. *J. Mol. Catal. A: Chem.* **2007**, *278*, 127.
(63) Huang, R.; Malizia, F.; Pennini, G.; Koning, C. E.; Chadwick, J. C. *Macromol. Rapid Commun.* **2008**, *29*, 1732.
(64) Sing, K. S. W.; Everett, D. H.; Haul, R. A. W.; Moscou, L.; Pierotti, R. A.; Rouquerol, J.; Siemieniewska, T. *Pure Appl. Chem.* **1985**, *57*, 603.
(65) Naik, B.; Parida, K. M.; Gopinath, C. S. *J. Phys. Chem. C* **2010**, *114*, 19473.
(66) (a) Reddy, A. S.; Gopinath, C. S.; Chilukuri, S. *J. Catal.* **2006**, *243*, 278. (b) Velu, S.; Suzuki, K.; Vijayaraj, M.; Barman, S.; Gopinath, C. S. *Appl. Catal., B* **2005**, *55*, 287.